Available online at www.sciencedirect.com
SCIENCE DIRECT
Chemical Physics Letters 420 (2006) 199–203
CHEMICAL PHYSICS LETTERS
www.elsevier.com/locate/cplett

Dissecting the stabilization of iodide at the air–water interface into components: A free energy analysis

Georgios Archontis [a,*], Epameinondas Leontidis [b]

[a] Department of Physics, University of Cyprus, Kallipoleos 75, PO20537, Nicosia CY1678, Cyprus
[b] Department of Chemistry, University of Cyprus, Kallipoleos 75, PO20537, Nicosia CY1678, Cyprus

Received 14 November 2005
Available online 19 January 2006

Abstract

Recent experiments and simulations show that large chaotropic anions favor solvation at the water surface, mainly due to induction interactions dominated by ionic polarizabilities. We compare the solvation free-energy components of iodide at the water surface and bulk with a recent, polarizable force field. The bulk position is stabilized by the interaction between the iodide permanent charge and the solvent permanent dipole moments; the surface is favored by the iodide polarizability and the reduced cavity accommodating the solute. The ionic solvation is not described satisfactorily by linear response; the non-linearity of the iodide induced dipole moment is discussed.

1. Introduction

The adsorption of ions at interfaces plays an important role in colloid and materials science [1,2], biological systems [3,4], atmospheric and environmental processes [5]. Early work by Onsager [6] had concluded that ions are excluded from the water surface, due to repulsion caused by electrostatic image forces. This argument was supported by early simulations with non-polarizable force fields [7]. However, simulations of water clusters [8–12], and planar water–air interfaces [13–21] with polarizable models, as well as modern spectroscopic methods [17,22–25] have provided evidence that many ions accumulate at the free water surface.

In earlier work [16] we employed a recent polarizable model for water [26] and ions [27] to simulate the air–water interface of an 1.2 M aqueous NaI solution and showed that the iodides were attracted at the surface with sodium in an adjacent, interior layer. The model simulates atomic polarizabilities with Drude particles and permits a transparent partitioning of the total ion–water interaction energy into components due to permanent and induced charges. Here, we exploit this property and decompose the solvation free energy of iodide at the water surface and the bulk into contributions due to permanent charges, induced charges and van der Waals interactions. The results provide insights into the reported correlation between the ionic charge, polarizability, or size and the propensity for the water surface [12,15,17]; furthermore, they constitute an additional test of the force field [26,27]. A linear response approximation fails to reproduce the solvation free energies, partly due to the non-linear dependence of the solute dipole moment on the solute induced charge.

2. Model and simulation methods

2.1. Model and simulation system

The water ('SWM4-DP' model [26,28]) and iodide parameters [27] have been reported in our earlier work [16]. A systematic development of a polarizable force field based on Drude oscillators is initiated in [29]. A cubic,

* Corresponding author. Fax: +357 22 332821.
E-mail address: archonti@ucy.ac.cy (G. Archontis).

0009-2614/$ - see front matter © 2005 Elsevier B.V. All rights reserved.
doi:10.1016/j.cplett.2005.12.051

31.05 Å solution of 1000 water molecules and a single iodide was simulated under periodic conditions in a tetragonal unit cell of dimensions $31{:}05 \times 31{:}05 \times 93{:}3$ Å^3, corresponding to a solution slab with two interfaces. All calculations employed the program CHARMM [30]. Details of the system and simulation methodology are supplied in [16].

2.2. Free-energy calculations

The calculations are summarized in the thermodynamic cycle of Fig. 1. The relative solvation free energy of the fully charged and polarizable iodide at the surface with respect to the bulk is equal to

$$\begin{aligned}\Delta\Delta A &= \Delta A_{\mathrm{s}} - \Delta A_{\mathrm{b}} \\ &= \Delta A_1 + \Delta A_{3\mathrm{S}} + \Delta A_{2\mathrm{S}} - \Delta A_{3\mathrm{B}} - \Delta A_{2\mathrm{B}} \end{aligned} \quad (1)$$

All free energy differences are explained in the legend of Fig. 1. Throughout the thermodynamic cycle we have used the *full* polarizable potential for the solvent [26].

Step 1: The transfer of the LJ particle from the surface to the bulk was accomplished by applying a harmonic restraint potential with a force constant $k = 4$ kcal/mol/Å^2 at the particle center. The reference points were $\vec{r}_{0,i} = (0, 0, z_i)$, with z_i varying between 14.5 and 0.0 Å in steps of 0.25 Å. The plane $z = 14.5$ Å (at the surface) is consistent with the single-ion simulations and energetic analysis in [16]. For each point we conducted a 100–150 ps simulation, with the first 30 ps treated as equilibration. The total simulation length was 6.75 ns. The total, unbiased probability $p(\vec{r})$ was obtained as described in [31]. The free-energy profile (Fig. 2) is $\Delta A(z) \equiv -k_{\mathrm{B}}T \ln[p(0,0,z)/p(0,0,14.5)]$.

Steps 2 and 3: The ion was restrained at $z = 0$ and $z = 14.5$ Å by a harmonic potential, with a constant of 7 kcal/mol/Å^2. In step 2, the solute permanent charge was switched on linearly, using a coefficient λ_{p} with values 0, 0.125, 0.25, 0.375, 0.5, 0.625, 0.75, 0.875 and 1.0. In step 3, the induced charges on iodide and its Drude were multiplied by a coefficient λ_{i} set to 0.125, 0.25, 0.375, 0.5, 0.625, 0.75, 0,8125, 0.875, 0.9375 and 1.0. For each $\lambda_{\mathrm{p,i}}$ value we conducted a 700 ps simulation and analyzed the last 500 ps.

The free-energies were calculated by the linear-scaling thermodynamic integration expressions

$$\begin{aligned}\Delta A_2 = \int_0^1 \mathrm{d}\lambda_{\mathrm{p}} \langle E_{\mathrm{I_pW_p}} \rangle_{\lambda_{\mathrm{p},0}} + \int_0^1 \mathrm{d}\lambda_{\mathrm{p}} \langle E_{\mathrm{I_pW_i}} \rangle_{\lambda_{\mathrm{p},0}} = \Delta A_{\mathrm{I_pW_p}} \\ + \Delta A_{\mathrm{I_pW_i}} \end{aligned} \quad (2)$$

$$\begin{aligned}\Delta A_3 = \int_0^1 \mathrm{d}\lambda_{\mathrm{i}} \langle E_{\mathrm{I_iW_p}} \rangle_{1,\lambda_{\mathrm{i}}} + \int_0^1 \mathrm{d}\lambda_{\mathrm{i}} \langle E_{\mathrm{I_iW_i}} \rangle_{1,\lambda_{\mathrm{i}}} = \Delta A_{\mathrm{I_iW_p}} \\ + \Delta A_{\mathrm{I_iW_i}} \end{aligned} \quad (3)$$

'I' and 'W' denote iodide and water, 'p', 'i' the permanent and induced charge and $\langle \cdots \rangle_{x,y}$ expectation values with $\lambda_{\mathrm{p}} = x$, $\lambda_{\mathrm{i}} = y$. $E_{\mathrm{I_pW_{p/i}}}$ (in ΔA_2) are the interaction energies between the fully charged, non-polarizable iodide and the water permanent/induced dipole moment; $\langle E_{\mathrm{I_pW_{p/i}}} \rangle_{\lambda_{\mathrm{p},0}}$ are the corresponding free-energy derivatives. Similarly, $E_{\mathrm{I_iW_{p/i}}}$ (in ΔA_3) are the interaction energies between the iodide induced dipole moment and the water permanent/induced dipole moment (with the iodide polarizability fully switched on, $\lambda_{\mathrm{i}} = 1$). The last equalities in Eqs. (2) and (3) define the free-energy components.

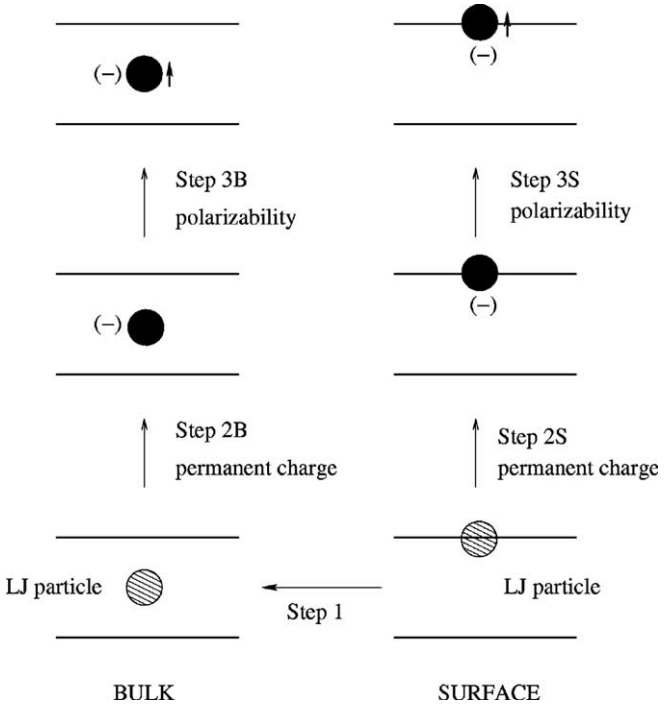

Fig. 1. Thermodynamic cycle employed in the free energy calculations. Step 1 corresponds to transferring a particle with the iodide Lennard-Jones (LJ) parameters [16] from the surface to the center of the slab. Steps 2B and 2S correspond to introducing a permanent charge $q = -1$ into the iodide at the center (B) or at the surface (S). Steps 3B and 3S correspond to introducing the induced charges (polarizability) onto the iodide particle and its Drude partner. The iodide Drude particle is not shown.

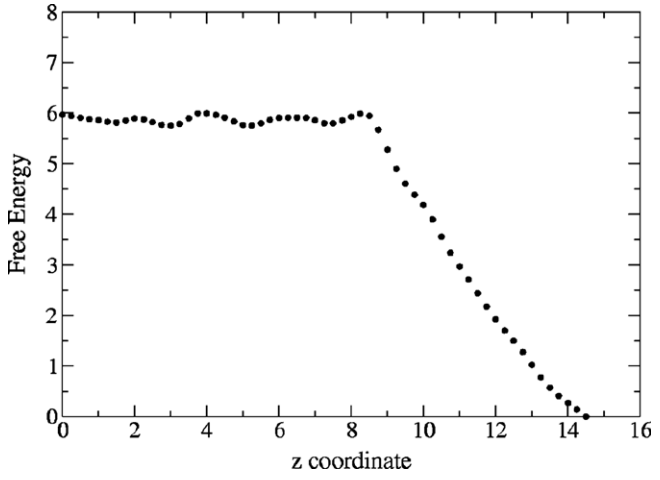

Fig. 2. Free energy profile associated with transferring a LJ particle with the iodide parameters [16] from the surface ($z = 14.5$) to the bulk position ($z = 0$) of the water slab.

2.3. Linear response approximation (LRA)

The free energy components of steps 2 and 3 were also computed by the LRA equation [32,33]

$$\Delta A^{\mathrm{LR}}_{\mathrm{I}_x\mathrm{W}_y} = \frac{1}{2}\left[\langle E_{\mathrm{I}_x\mathrm{W}_y}\rangle_{\mathrm{LJ}} + \langle E_{\mathrm{I}_x\mathrm{W}_y}\rangle_{\mathrm{I,\ P}}\right] \quad (4)$$

where 'LJ' and 'I, P' denote, respectively, the LJ-particle end-state and the fully charged, fully polarizable iodide end-state. For the 'I, P' averages we used the trajectories from the end of step 3 ($\lambda_p = \lambda_i = 1$). The 'LJ' averages were computed by simulations, in which the solute model consisted of the (uncharged) iodide and its Drude site.

3. Results

3.1. Free energy calculations

The free energy profile of the LJ particle (step 1) is shown in Fig. 2; the curve has been translated to pass through 0.0 at $z = 14.5$ Å. In the region $z = 14.5$–8.5 Å, the free-energy increases steadily from 0.0 to 5.9 kcal/mol, reflecting the tendency of the aqueous phase to reduce the solute-accommodating cavity by expelling the hydrophobic particle. The LJ particle–water oxygen radial distribution function (rdf) with the solute restrained at $z = 8.5$ Å has a second hydration shell starting at 6 Å, roughly the distance from the surface where the profile plateau appears (all rdf's are discussed in Supplementary Material). Thus, the free energy becomes insensitive to the solute position when the second hydration shell of the LJ particle starts to form.

The results of all steps are summarized in Table 1. Introduction of the iodide permanent charge (step 2) stabilizes the bulk by 5.3 kcal/mol, relative to the surface, due to the interaction with the *permanent* water dipole moment (component $\Delta A_{\mathrm{I_pW_p}}$). The solute polarizability (step 3) stabilizes the surface position by 1.9 kcal/mol. The largest contribution comes from the interaction with the water permanent dipole moment (component $\Delta A_{\mathrm{I_iW_p}}$).

From the three steps and Eq. (1) it follows that the net stabilization of the surface position is 2.5 kcal/mol. The contribution from the solute polarizability is 1.9 kcal/mol, the rest coming from the smaller free energy needed to create a partial solute cavity at the surface (step 1). Note that the charged, non-polarizable solute is still preferentially solvated at the surface by 0.6 kcal/mol ($=\Delta A_{2S} - \Delta A_{2B} - \Delta A_1$). This may be in part because the combination of LJ and permanent/induced charges are optimal for the fully charged and polarizable iodide [27]. Nevertheless, simulations of a NaI solution with a different polarizable water and *non*-polarizable iodide model also resulted in the accumulation of iodide at the surface [15]. The free energy profile of the fully charged, polarizable iodide across the water/vapor interface was computed in [13] by a different water and solute model, yielding a surface minimum with a well depth of 1.5 kcal/mol.

Ionic concentration profiles obtained from simulations with an 1.2 M NaI electrolyte solution [14,16] suggest a stabilization of the surface site by only ≈0.5 kcal/mol. This smaller value could be partly attributed to the existence of a double charge layer in the electrolyte solution [14,16,22], i.e. to a repulsion between iodide ions at the surface, combined with an attraction of iodides toward the bulk due to the interior sodium layer.

Table 1
Free energy results[a]

Step	Free energy component[b]	Bulk	Surface	Difference
1	pmf	0.0[c]	5.9 (0.1)	−5.9 (0.1)
2	$\Delta A_{\mathrm{I_pW_p}}$	−54.2 (0.1)	−48.7 (0.1)	5.5 (0.1)
2	$\Delta A_{\mathrm{I_pW_i}}$	−10.9 (0.1)	−11.1 (0.1)	−0.2 (0.1)
2	Total	−65.1(0.1)	−59.8 (0.1)	5.3 (0.2)
3	$\Delta A_{\mathrm{I_iW_p}}$	−2.4 (0.1)	−3.9 (0.1)	−1.5 (0.1)
3	$\Delta A_{\mathrm{I_iW_i}}$	−0.41 (0.03)	−0.75 (0.03)	−0.34 (0.1)
3	Total	−2.8 (0.1)	−4.7 (0.1)	−1.9 (0.2)
2 + 3				+3.5 (0.3)
1 + 2 + 3				−2.4 (0.3)

[a] All free energies in kcal/mol. Free-energy component errors (in parentheses) correspond to the standard deviation of the results, obtained by partitioning the data into 4 groups.

[b] 'I' and 'W' denote, respectively, iodide and water; 'p' and 'i' denote permanent and induced charge (see also text). Total errors are evaluated by error propagation. The free energy components are defined in Eqs. (2) and (3).

[c] The profile is translated to pass through zero at this point.

3.2. Comparison with the estimates from a linear response approximation

A linear response hypothesis is often used for the rapid calculation of free-energy differences [34,33], but is not satisfied by the polarizable model employed here. The free energy derivatives (shown in Fig. 3) do not depend linearly on $\lambda_{\mathrm{p,i}}$; the largest deviation is observed in step 3. The LRA estimates of the free-energy components are in Table 2. Components $\Delta A^{\mathrm{LR}}_{\mathrm{I_iW_p}}$ and $\Delta A^{\mathrm{LR}}_{\mathrm{I_iW_i}}$ differ from the exact values by 250%/150% (bulk/surface) and 320%/100%, respectively. The deviations cancel to some extent in the double free-energy differences.

The average iodide dipole moment depends on the scaling parameter λ_i as

$$\langle p_{\mathrm{ind,I}}\rangle = \alpha_{\mathrm{I}}\langle E(\lambda_i)\rangle = \frac{\lambda_i^2 q_{\mathrm{ind,I}}}{k_{\mathrm{I}}}\left(c_0 + c_1\lambda_i + c_2\lambda_i^2 + \cdots\right)\rangle \quad (5)$$

with $\alpha_{\mathrm{I}} = \lambda_i^2 q_{\mathrm{ind,I}}/k_{\mathrm{I}}$ [26] the iodide polarizability, k_{I} the Drude-oscillator force constant and $\langle E(\lambda_i)\rangle$ the average electric field at the solute, when the iodide induced charge is $\lambda_i q_{\mathrm{ind,I}}$; the second equality assumes a Taylor expansion of $\langle E(\lambda_i)\rangle$ around $\lambda_i = 0$. Eq. (5) shows that the iodide dipole moment $\langle p_{\mathrm{ind,I}}\rangle$ is a polynomial of λ_i. The quantity $\langle p_{\mathrm{ind,I}}\rangle$ is reproduced well by a fourth-order polynomial

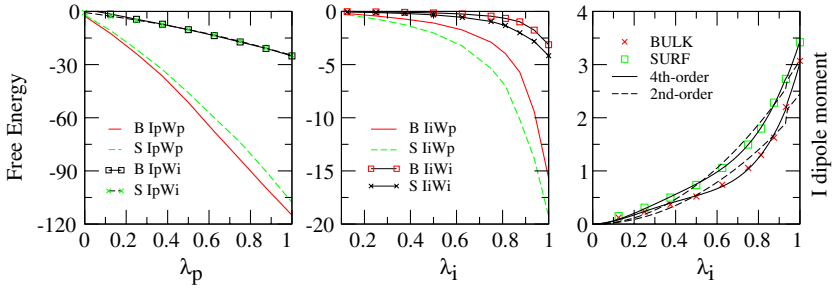

Fig. 3. Free energy derivatives for step 2 (left) and step 3 (middle), as a function of the permanent or induced charge scaling parameter. 'B' and 'S' correspond to bulk/surface. (Right): Average iodide dipole moment as a function of the induced-charge scaling parameter λ_i (step 3). The dipole moment is fitted with high accuracy to a fourth-order polynomial of λ_i (see Eq. (4)).

Table 2
Linear response estimation of the free energy components in steps 2 and 3[a] (Eq. (4))

Term[b]	Bulk				Surface				$\Delta\Delta G$	
	LJ[c]	I, P[c]	LR[d]	Ex[e]	LJ[c]	I, P[c]	LR[d]	Ex[e]	LR[d]	Ex[e]
$\langle E_{I_pW_p}\rangle$	−2.6	−114.3	−58.5	−54.2	−2.2	−107.3	−54.8	−48.7	+3.7	+5.5
$\langle E_{I_pW_i}\rangle$	1.2	−27.3	−13.0	−10.9	−0.4	−28.6	−14.5	−11.1	−1.5	−0.2
$\langle E_{I_iW_p}\rangle$	0.0	−16.9	−8.5	−2.4	0.0	−19.3	−9.7	−3.9	−1.2	−1.5
$\langle E_{I_iW_i}\rangle$	0.0	−3.3	−1.7	−0.4	0.0	−4.2	−2.1	−0.8	−0.4	−0.4
Total	−1.4	−161.8	−81.7	−67.9	−2.8	−159.4	−81.1	−64.5	0.6	+3.4

[a] All values in kcal/mol.
[b] See Eq. (4).
[c] 'LJ' and 'I, P' denote, respectively, the LJ-particle and the fully charged, polarizable solute end-state.
[d] Average over the 'LJ' and 'I, P' end states.
[e] Exact free energy components (from Table 1).

of λ_i (Fig. 3, right panel), highlighting the importance of terms beyond linear order in Eq. (5) and explaining the deviation from LR in step 3. We note that the *solvent* induced dipole moment has a very small dependence on the solute permanent (step 2) or induced (step 3) charge (data not shown).

4. Conclusions

Our free-energy decomposition results are in accordance with the reported correlation between surface attraction and solute size/polarizability [12,15], and provide a quantitative framework to understand the behavior of ions at the free water surface. Small-size, weakly polarizable solutes (e.g., cations) avoid the surface because the cavity and induction contributions cannot overcome the free energy gain associated with introducing the solute permanent charge in the bulk; the opposite occurs in the case of larger, more polarizable solutes. When cavity and direct charge interactions almost balance each other, the induction interactions play a critical role, driving the ions to the surface. The role of ionic polarizability is found to be crucial, without the need to postulate additional dispersion interactions between the ion and the air–water interface [35]. The ionic polarizability is consistently higher at the surface (Fig. 3, right panel) due to the asymmetrical solvent distribution around the ion [13,15,16], leading to stronger solute–solvent interactions and a tighter first solvation shell.

Acknowledgements

We thank Guillaume Lamoureux and Benoit Roux, for the iodide parameters. Simulations were performed on a Linux cluster, partly funded by Grant RPF/ERYAN/0603 (to G.A.). This research was partly funded by a "Program for the Support of Young Researchers" (PENEK/Integration) grant to G.A. and E.L.

Appendix A. Supplementary data

Supplementary data associated with this article can be found, in the online version, at doi:10.1016/j.cplett.2005.12.051.

References

[1] J. Lyklema, Fundamentals of Interface and Colloid Science, vol. II, Academic Press, London, 1995.
[2] E. Leontidis, Curr. Opin. Colloid Interf. Sci. 7 (2002) 81–91.
[3] M.G. Cacace, E.M. Landau, J.J. Ramsden, Quart. Rev. Biophys. 30 (1997) 241–277.
[4] R.L. Baldwin, Biophys. J. 71 (1996) 2056–2063.
[5] E.M. Knipping, M.J. Lakin, K.L. Foster, P. Jungwirth, D.J. Tobias, R.B. Gerber, D. Dabdub, B. Finlayson-Pitts, Science 288 (2000) 301–306.
[6] L. Onsager, N.N.T. Samaras, J. Chem. Phys. 2 (1934) 528–536.
[7] M. Wilson, A. Pohorille, J. Chem. Phys. 95 (1991) 6005–6013.
[8] L. Perera, M.L. Berkowitz, J. Chem. Phys. 96 (1992) 8288–8294.
[9] L.X. Dang, B.C. Garrett, J. Chem. Phys. 99 (1993) 2972–2977.
[10] S.J. Stuart, B.J. Berne, J. Phys. Chem. A 103 (1999) 10300.

[11] G.H. Perlherbe, B.M. Ladanyi, J.T. Hynes, Chem. Phys. 258 (2000) 201–224.
[12] D.H. Herce, L. Perera, T.A. Darden, C. Sagui, J. Chem. Phys. 122 (2005) 024513.
[13] L.X. Dang, T.-M. Chang, J. Phys. Chem. B 106 (2002) 235–238.
[14] P. Jungwirth, D.J. Tobias, Phys. Chem. B 106 (2002) 6361–6373.
[15] L. Vrbka, M. Mucha, B. Minofar, P. Jungwirth, E.C. Brown, D.J. Tobias, Curr. Opin. Colloid Interf. Sci. 9 (2004) 67–73.
[16] G. Archontis, E. Leontidis, G. Andreou, J. Phys. Chem. B 38 (2005) 17957–17966.
[17] E.C. Brown, M. Mucha, P. Jungwirth, D.J. Tobias, J. Phys. Chem. B 109 (2005) 7934–7940.
[18] M. Mucha, T. Frigato, L.M. Levering, H.C. Allen, D.J. Tobias, L.X. Dang, P. Jungwirth, J. Phys. Chem. B 109 (2005) 7617–7623.
[19] S. Gopalakrishnan, P. Jungwirth, D.J. Tobias, H.C. Allen, J. Phys. Chem. B 109 (2005) 8861–8872.
[20] P.B. Petersen, R.J. Saykally, M. Mucha, P. Jungwirth, J. Phys. Chem. B 109 (2005) 10915–10921.
[21] M. Roeselova, J. Vieceli, L.X. Dang, B.C. Garrett, D.J. Tobias, J. Am. Chem. Soc. 126 (2004) 16308–16309.
[22] M.J. Shultz, S. Baldelli, C. Schnitzer, D. Simonelli, J. Phys. Chem. B 10 (2002) 5313–5324.
[23] P.B. Petersen, R.J. Saykally, Chem. Phys. Lett. 397 (2004) 51–55.
[24] D. Liu, G. Ma, L.M. Levering, H.C. Allen, J. Phys. Chem. B 108 (2004) 2252–2260.
[25] S. Ghosal, J. Hemminger, H. Bluhm, B. Mun, E.L.D. Hebenstreit, G. Ketteler, D.F. Ogletree, F.G. Requejo, M. Salmeron, Science 307 (2005) 563–566.
[26] G. Lamoureux, A.D. Mackerell, B. Roux, J. Chem. Phys. 119 (2003) 5185–5197.
[27] G. Lamoureux, B. Roux, submitted for publication.
[28] G. Lamoureux, B. Roux, J. Chem. Phys. 119 (2003) 3025–3039.
[29] V.M. Anisimov, G. Lamoureux, I.V. Vorobyov, N. Huang, B. Roux, A.D. Mackerell, J. Chem. Theory Comput. 1 (2005) 153–168.
[30] B.R. Brooks, R.E. Bruccoleri, B.D. Olafson, D.J. States, S. Swaminathan, M. Karplus, J. Comput. Chem. 4 (1983) 187–217.
[31] T.B. Woolf, B. Roux, J. Am. Chem. Soc. 116 (1994) 5919–5926.
[32] J. Aqvist, C. Medina, J.-E. Samuelson, Protein Eng. 8 (1995) 1137–1144.
[33] G. Archontis, T. Simonson, Biophys. J. 88 (2005) 3888–3904.
[34] J. Aqvist, V.B. Luzhkov, B.O. Brandsal, Accounts Chem. Res. 35 (2002) 358–365.
[35] D. Boström, D.R.M. Williams, B.W. Ninham, Langmuir 17 (2001) 4475–4478.